P. P. Wang
O. S. Spencer

Threshold Voltage Characteristics of Double-boron-implanted Enhancement-mode MOSFETs

Abstract: Threshold voltage characteristics are presented for a double boron-ion-implanted n-channel enhancement MOSFET device for high speed logic circuit applications. A 15-Ω-cm high resistivity p-type (100) substrate was used to achieve low junction capacitance and low threshold substrate sensitivity. A shallow boron implant was used to raise the threshold voltage, and a second, deeper, boron implant was used to increase the punch-through voltage between the source and the drain. This design is especially beneficial for short channel devices, while maintaining the low junction capacitance and low threshold substrate sensitivity of the high resistivity substrate. A one-dimensional analysis was performed to predict the effects of ion implantation dose and energy on the device characteristics, and a quasi two-dimensional analysis was used to account for the short channel effect. The calculated results agree well with the behavior of experimental devices fabricated in the laboratory.

Introduction

Boron ion implantation to control the threshold voltage of n-channel enhancement MOSFETs has been discussed [1–6]. The ability to control the surface dopant concentration by ion implantation allows use of a high resistivity wafer material. The chief advantage of this is the extra depletion region width for a given applied voltage, leading to a lower junction capacitance and a reduction in the dependency of substrate potential on the threshold voltage (threshold substrate sensitivity). Both are important considerations for digital circuit switching speed. However, the source-drain punch-through voltage is reduced in the high resistivity substrate, especially for smaller channel length devices. A handy solution for this problem is the deep implantation of boron (in an n-channel device), which raises the punch-through voltage with minimal effect on the substrate sensitivity [7]. Thus, by using a double ion implantation, one shallow and one deep (corresponding to a low and a high implant energy) of the same species, the advantages of a high resistivity substrate can be enjoyed, with the disadvantages minimized or eliminated [8].

Ion implantation allows considerable freedom as far as attaining specific results is concerned but makes device characterization more difficult. Of course, numerical methods [9–11] can be used but these are cumbersome and offer little insight into the contributions of the various factors in the final solution.

This paper describes analytical approximations that have been found to adequately represent the threshold voltage characteristics for a double ion implanted MOSFET. One approximation reduces the complicated doping profile of an ion implanted MOSFET to two uniformly doped layers (a step profile) on a uniform substrate [3–5]. Another approximation considers the ion implanted dopant distribution to be Gaussian and assumes the depletion region boundary to be in the semiconductor bulk. In all of these analyses, the effect of short channels on the device characteristics is taken into consideration by modifying the approach used by Poon, et al. [12] and by Yau [13]. In this paper, much of the complex mathematics is provided in an appendix.

The experimental results were obtained from devices fabricated in our laboratory. The substrate material is 15-Ω-cm (100) p-type silicon with a 500-Å oxide and an aluminum gate. The vertical structure of this fabricated device is shown in Fig. 1. Junction depths of the source/drain are typically 1.7 μm. Double energy boron ion

Table 1 Double boron ion implantation characteristics.

Implant	*Dose* (atoms/cm^2)	*Energy* (keV)	*Range*[a] (Å)	*Straggle* (Å)
Shallow	6×10^{11}	35	655	361
Deep	2×10^{11}	150	3665	716

[a]Oxide thickness has been deducted.

implantation is used to tailor the gate region for an enhancement device, thus yielding a double-peaked doping profile, as shown in Fig. 2. The shallow implant is 6×10^{11} atoms/cm^2 at 35 keV, whereas the deep implant is 2×10^{11} atoms/cm^2 at 150 keV. The nominal channel length of these devices is about 3 μm.

Step profile approximation

Assume that the implanted ion distribution is Gaussian, namely [14–16],

$$N \exp\,[-(x-\bar{x})^2/2\sigma^2],$$

where $\bar{x}$ is the range, σ is the "straggle," and $N = \Phi/\sigma(2\pi)^{\frac{1}{2}}$ is the maximum concentration of ions/cm^3 (Φ = ion dose). Therefore, the nonuniform doping profile for this double boron-implanted device has the form

$$C(x) = N_B + \sum_{i=1,\,2} N_i \exp[-(x-\bar{x}_i)^2/2\sigma_i^2], \tag{1}$$

where N_B is substrate concentration and subscripts 1 and 2 refer to the shallow and deep implants, respectively. The characteristics for both implants are given in Table 1.

Instead of considering the nonuniform double Gaussian profile, we replace profile $C(x)$ with a two-step profile, as shown in Fig. 2. Here N_{AS} and N_{AB} are the average shallow and deep implanted concentrations, namely,

$$N_{AS} = \frac{1}{W_S}\int_0^{W_S} N_1 \exp[-(x-\bar{x}_1)^2/2\sigma_1^2]\,dx \tag{2}$$

and

$$N_{AB} = \frac{1}{W_B}\int_{W_S}^{W_S+W_B} N_2 \exp[-(x-\bar{x}_2)^2/2\sigma_2^2]\,dx, \tag{3}$$

where W_S and W_B are the widths of the step doping profiles and have the forms

$$W_S = \bar{x}_1 + 2\sigma_1, \tag{4}$$

$$W_B = (\bar{x}_2 - \bar{x}_1) + 2(\sigma_2 - \sigma_1). \tag{5}$$

Because W_S is about 1300 Å, the depletion region boundary at source-to-substrate voltage $V_{sx} = 0$ always lies beyond W_S (the thickness of the shallow implant). We want to consider two different cases.

In the first case, the depletion boundary is located within the deep implant region, i.e., $W_s < x_{dm} < W_s + W_B$. The maximum depletion region thickness can be written as

$$x_{dm} = \left\{\frac{2\epsilon_s}{q(N_{AB}+N_B)}\left[\phi_{so} + |V_{sx}| - \frac{q(N_{AS}-N_{AB})W_S^2}{2\epsilon_s}\right]\right\}^{\frac{1}{2}}, \tag{6}$$

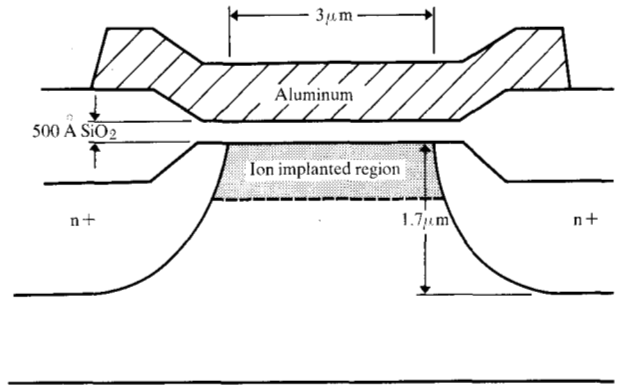

Figure 1 Double-boron-implanted enhancement n-channel MOSFET device structure. Shallow implant concentration is 6×10^{11} atoms/cm^2 at 35 keV; deep implant concentration is 2×10^{11} atoms/cm^2 at 150 keV. Substrate material is 15-Ω-cm p-type silicon, and substrate concentration N_B is 10^{15} atoms/cm^3.

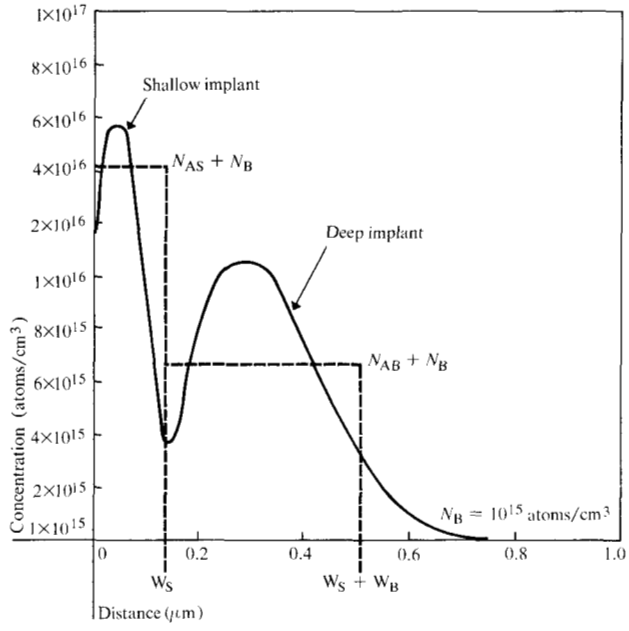

Figure 2 Theoretical ion implant profile and step profile approximation for concentrations given for Fig. 1.

where ϵ_s is the permittivity of silicon and ϕ_{so} is silicon surface potential at the onset of strong inversion. Thus,

$$V_{bulk} = \frac{q(N_{AS}-N_{AB})W_S}{C_{ox}} + \frac{q(N_{AB}+N_B)x_{dm}}{C_{ox}}, \tag{7}$$

where C_{ox} is gate dielectric capacitance. The threshold voltage V_T is

$$V_T = V_{FB} + \phi_{so} + \frac{q(N_{AS} - N_{AB})W_S}{C_{ox}} + \frac{[2\epsilon_s q(N_{AB} + N_B)]^{\frac{1}{2}}}{C_{ox}} \left[\phi_{so} + |V_{sx}| - \frac{q(N_{AS} - N_{AB})W_S^2}{2\epsilon_s}\right]^{\frac{1}{2}}, \quad (8)$$

where V_{FB} is flat band voltage. This follows directly from Eqs. (A7), (A10), and (A9) of the appendix. It can be seen from this expression that the effect of the implanted profile on the threshold voltage is two-fold. A linear shift $q(N_{AS} - N_{AB})W_S/C_{ox}$ is accompanied by a modification of the $|V_{sx}|$ term under the square root, $-q(N_{AS} - N_{AB})W_S^2/2\epsilon_s$. The latter term affects the dependence of threshold voltage on the source-to-substrate voltage. Note that both terms depend on the difference between the two average implant concentrations, $N_{AS} - N_{AB}$.

In the second case, $x \geq W_S + W_B$, the depletion boundary is in the bulk region, beyond the deep implant region, yielding

$$x_{dm} = \left\{\frac{2\epsilon_s}{qN_B}\left[\phi_{so} + |V_{sx}| - \frac{qN_{AS}W_S^2}{2\epsilon_s} - \frac{qN_{AB}(W_B^2 + 2W_BW_S)}{2\epsilon_s}\right]\right\}^{\frac{1}{2}}, \quad (9)$$

and

$$V_{bulk} = \frac{q(N_{AS}W_S + N_{AB}W_B)}{C_{ox}} + \frac{qN_Bx_{dm}}{C_{ox}}. \quad (10)$$

Thus,

$$V_T = V_{FB} + \phi_{so} + \frac{q(N_{AS}W_S + N_{AB}W_B)}{C_{ox}} + \frac{(2\epsilon_s qN_B)^{\frac{1}{2}}}{C_{ox}}\left[\phi_{so} + |V_{sx}| - \frac{qN_{AS}W_S^2}{2\epsilon_s} - \frac{qN_{AB}(W_B^2 + 2W_BW_S)}{2\epsilon_s}\right]^{\frac{1}{2}}. \quad (11)$$

We see that the nonuniform doping profile shifts the threshold by an amount

$$\frac{q(N_{AS}W_S + N_{AB}W_B)}{C_{ox}}$$

and modifies the substrate voltage by an amount

$$-\frac{qN_{AS}W_S^2}{2\epsilon_s} - \frac{qN_{AB}(W_B^2 + 2W_BW_S)}{2\epsilon_s}.$$

The term $(N_{AS}W_S + N_{AB}W_B)$ represents the total dosage of boron implanted into the silicon from both the deep and shallow implants.

Let us now consider the intrinsic band bending at the silicon surface at the onset of strong inversion. As used by Doucet and Van de Weile [17] the surface inversion condition is dictated by the doping concentration of the depletion edge. Because there is a discontinuity in the step profile approximation at $x_{dm} = W_S + W_B$, there is also a discontinuity in the strong inversion criterion. Nevertheless, the step profile approximation offers a simple and direct first-order understanding of the influence of shallow and deep channel ion implantation doses and energies on the threshold voltage and its dependence on the source-to-substrate voltage.

We define a critical substrate voltage V_c as the voltage for which the depletion boundary is located at $W_S + W_B$, the interface between the shallow and deep implants. From Eq. (9), setting $x_{dm} = W_S + W_B$ and solving for $|V_{sx}|$, one obtains

$$V_c = \frac{qN_{AS}W_S^2}{2\epsilon_s} + \frac{qN_{AB}(W_B^2 + 2W_BW_S)}{2\epsilon_s} + \frac{qN_B(W_S + W_B)^2}{2\epsilon_s} - \phi_{so}. \quad (12)$$

For $|V_{sx}| < V_c$, the depletion boundary is located in the deep implant region, so Eqs. (6-8) are used. For $|V_{sx}| \geq V_c$, the depletion boundary is located in the uniformly doped substrate, so Eqs. (9-11) are used. In summary, we can conclude that the threshold has the general form

$$V_T = V_{FB} + \phi_{so} + \Delta V_T + \frac{(2\epsilon_s qN_X)^{\frac{1}{2}}}{C_{ox}}(\phi_{so} + |V_{sx}| + \Delta V_{sx})^{\frac{1}{2}}, \quad (13)$$

where

$$\phi_{so} = \begin{cases} 2kT/q \ln [(N_{AB} + N_B)/n_i] & \text{for } |V_{sx}| < V_c; \\ 2kT/q \ln (N_B/n_i) & \text{for } |V_{sx}| \geq V_c, \end{cases} \quad (13a)$$

$$V_{FB} = \begin{cases} \phi_{ms} - Q_{ox}/C_{ox} - kT/q \ln [(N_{AB} - N_B)/n_i] & \text{for } |V_{sx}| < V_c, \\ \phi_{ms} - Q_{ox}/C_{ox} & \text{for } |V_{sx}| \geq V_c, \end{cases} \quad (13b)$$

(ϕ_{ms} is the work function difference and is referred to the semiconductor bulk, Q_{ox} is the effective oxide charge, and n_i is silicon intrinsic concentration.)

$$N_X = \begin{cases} N_{AB} + N_B & \text{for } |V_{sx}| < V_c, \\ N_B & \text{for } |V_{sx}| \geq V_c, \end{cases} \quad (13c)$$

$$\Delta V_T = \begin{cases} \frac{q(N_{AS} - N_{AB})W_S}{C_{ox}} & \text{for } |V_{sx}| < V_c, \\ \frac{q(N_{AS}W_S + N_{AB}W_B)}{C_{ox}} & \text{for } |V_{sx}| \geq V_c, \end{cases} \quad (13d)$$

$$\Delta V_{sx} = \begin{cases} -\dfrac{q(N_{AS} - N_{AB})W_S^2}{2\epsilon_s} & \text{for } |V_{sx}| < V_c, \\ -\dfrac{qN_{AS}W_S^2}{2\epsilon_s} - \dfrac{qN_{AB}(W_B^2 + 2W_BW_S)}{2\epsilon_s} & \text{for } |V_{sx}| \geq V_c. \end{cases} \quad (13e)$$

Gaussian implant profile approximation

Now we want to use the nonuniform profile $C(x)$ in Eq. (1) to calculate x_{dm}, V_{bulk}, and V_T. As indicated previously, at $|V_{sx}|$ greater than V_c, the depletion boundary x_{dm} is located in the bulk substrate region. Therefore, we can neglect the term in (A7) due to nonuniformity in the doping concentration, namely, $x_{dm}\ (d\phi/dx)_{x_{dm}}$ This may introduce some error as $|V_{sx}|$ approaches V_c, but because the devices described here operate at $|V_{sx}| = 5$ V, the above error is not important. A solution of Poisson's equation, as discussed in the appendix, leads to

$$\phi_{so} + |V_{sx}| = \frac{qN_B x_{dm}^2}{2\epsilon_s} + \frac{q}{\epsilon_s}\sum_{i=1,2} N_i J_i(x_{dm}),$$

where

$$J_i(x_{dm}) = \int_0^{x_{dm}} x \exp[-(x - \bar{x}_i)^2/2\,\sigma_i^2]\,dx. \quad (14)$$

The calculation of the integral J_i $(i = 1, 2)$ is done in the usual way, the value being

$$J_i = \frac{\bar{x}_i\sigma_i\,(2\pi)^{\frac{1}{2}}}{2}\left[\operatorname{erf}\left(\frac{x_{dm} - \bar{x}_i}{2^{\frac{1}{2}}\sigma_i}\right) + \operatorname{erf}\left(\frac{\bar{x}_i}{2^{\frac{1}{2}}\sigma_i}\right)\right] + \sigma_i^2\{\exp(-\bar{x}_i^2/2\sigma_i^2) + \exp[-(x_{dm} - \bar{x}_i)^2/2\sigma_i^2]\}. \quad (15)$$

At $|V_{sx}| \geq V_c$, $x_{dm} \geq \bar{x}_2 + 2\sigma_2$ (which is equal to $W_B + W_S$), and from Table 1, the above integrals reduce to very simple forms. For the shallow implant,

$$J_1 \approx \bar{x}_1\sigma_1\left(\frac{\pi}{2}\right)^{\frac{1}{2}}\left[1 + \operatorname{erf}\left(\frac{\bar{x}_1}{2^{\frac{1}{2}}\sigma_1}\right)\right] + \sigma_1^2\exp(-x_1^2/2\sigma_1^2), \quad (16)$$

and for the deep implant,

$$J_2 \approx \bar{x}_2\sigma_2\,(2\pi)^{\frac{1}{2}}. \quad (17)$$

By substituting Eqs. (16) and (17) into (14), the depletion boundary x_{dm} can be written as

$$x_{dm} = \left(\frac{2\epsilon_s}{qN_B}\left\{\phi_{so} + |V_{sx}| - \frac{q\Phi_2\bar{x}_2}{\epsilon_s} - \frac{q\Phi_1\bar{x}_1}{2\epsilon_s}\left[1 + \operatorname{erf}\left(\frac{\bar{x}_1}{2^{\frac{1}{2}}\sigma_1}\right)\right] - \frac{q\Phi_1\sigma_1}{(2\pi)^{\frac{1}{2}}\epsilon_s}\exp(-x_1^2/2\sigma_1^2)\right\}\right)^{\frac{1}{2}} \quad (18)$$

and V_{bulk} becomes

$$V_{bulk} = \frac{q}{C_{ox}}\sum_{i=1,2}^{2} N_i\int_0^{x_{dm}} \exp[-(x - \bar{x}_i)^2/2\sigma_i^2]\,dx. \quad (19)$$

The calculation of this integral is simple, and Eq. (19) reduces to

$$V_{bulk} \approx \frac{q\Phi_2}{C_{ox}} + \frac{q\Phi_1}{2C_{ox}}\left[1 + \operatorname{erf}\left(\frac{\bar{x}_1}{2^{\frac{1}{2}}\sigma_1}\right)\right] + \frac{qN_Bx_{dm}}{C_{ox}}. \quad (20)$$

Finally, the threshold voltage under the Gaussian implant profile approximation for the double boron implant enhancement MOSFETs gives

$$V_T = V_{FB} + \phi_{so} + \frac{q\Phi_2}{C_{ox}} + \frac{q\Phi_1}{2C_{ox}}\left[1 + \operatorname{erf}\left(\frac{\bar{x}_1}{2^{\frac{1}{2}}\sigma_1}\right)\right] + \frac{(2\epsilon_s qN_B)^{\frac{1}{2}}}{C_{ox}}\left\{\phi_{so} + |V_{sx}| - \frac{q\Phi_2\bar{x}_2}{\epsilon_s} - \frac{q\Phi_1x_1}{2\epsilon_s}\left[1 + \operatorname{erf}\left(\frac{\bar{x}_1}{2^{\frac{1}{2}}\sigma_1}\right)\right] - \frac{q\Phi_1\sigma_1}{(2\pi)^{\frac{1}{2}}\epsilon_s}\exp(-\bar{x}_1^2/2\sigma_1^2)\right\}^{\frac{1}{2}}. \quad (21)$$

By examining the above equation, one notes that the threshold voltage shifts by an amount ΔV_T due to both the shallow and deep ion implantations. The magnitude of the shift is

$$\Delta V_T = \frac{q\Phi_2}{C_{ox}} + \frac{q\Phi_1}{2C_{ox}}\left[1 + \operatorname{erf}\left(\frac{\bar{x}_1}{2^{\frac{1}{2}}\sigma_1}\right)\right]. \quad (22)$$

This shift corresponds to the total dose of the deep implant Φ_2 because almost all of the dose is in the silicon. However, only a fraction of the shallow implant is in the silicon, namely, $\frac{1}{2}[1 + \operatorname{erf}(\bar{x}_1/2^{\frac{1}{2}}\sigma_1)]$ of the total dose Φ_1, and thus only this amount contributes to the threshold shift. From Table 1, about 87 percent of the total shallow boron implant dose is in the silicon. The substrate voltage inside the square root of Eq. (21) also shifts by an amount

$$\Delta V_{sx} = -\frac{q\Phi_2\bar{x}_2}{\epsilon_s} - \frac{q\Phi_1\bar{x}_1}{2\epsilon_s}\left[1 + \operatorname{erf}\left(\frac{\bar{x}_1}{2^{\frac{1}{2}}\sigma_1}\right)\right] - \frac{q\Phi_1\sigma_1}{(2\pi)^{\frac{1}{2}}\epsilon_s}\exp(-\bar{x}_1^2/2\sigma_1^2). \quad (23)$$

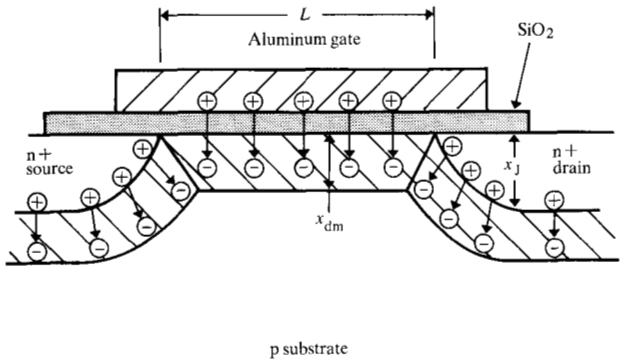

Figure 3 Short channel model structure due to Poon and Yau.

Table 2 Summary of step and Gaussian profile approximations for 500 Å gate oxide and $V_c = 1.19$ V. For the shallow implant, $N_{AS} = 4.10 \times 10^{16}$ atoms/cm^3 and $W_S = 1377$Å. For the deep implant, $N_{AB} = 5.25 \times 10^{15}$ atoms/cm^3 and $W_B = 3720$Å.

Approximation	$\lvert V_{sx}\rvert < V_c$		$\lvert V_{sx}\rvert \geq V_c$	
	ΔV_T (V)	ΔV_{sx}	ΔV_T (V)	ΔV_{sx}
Step profile	1.14	−0.52	1.76	−1.57
Gaussian profile	–	–	1.80	−1.74

The shifts in threshold voltage ΔV_T and substrate voltage ΔV_{sx} resulting from using the step profile approximation and the Gaussian implant profile approximation for double-boron-implanted enhancement n-channel MOSFETs are summarized in Table 2. It can be seen that the two approximations are in good agreement in the case $|V_{sx}| \geq V_c$.

Short channel effect

The equations for threshold voltage used in the preceding sections are valid as long as the channel length of the MOSFET is relatively long compared to the junction depths of the source and drain diffusions. An integral over $C(x)$, as in (A-10) of the appendix, represents the total charge Q_d within the depletion region. In the case of short channel devices, Q_d decreases from this value, because some of the electrical lines arising from charges near the source/drain are terminated on the source/drain, rather than the gate. Therefore, the doping level under the gate is effectively reduced, and the threshold voltage is lower than predicted. Recently, Lee [18, 19] derived a theory that indicates that the threshold voltage is, in general, a function of channel length, junction depth, and drain to source voltage. However, his expression is quite complicated and may not be suitable for computer aided design. To include the short channel effect, we adopted the approach used by Poon, et al. [12] and by Yau [13]. Without going through a two-dimensional analysis, the field lines arising from the depletion charge can be considered approximately as in Fig. 3. The field lines originating from the charges inside the trapezoidal depletion region are terminated on the gate electrode, whereas the field lines from the charge outside the trapezoidal region are terminated in the source/drain region. Based on this geometrical approximation, the effective depletion charge inside the trapezoidal area is

$$Q_{d(\text{eff})} = F \int_0^{x_{dm}} C(x)\, dx. \tag{24}$$

The form factor F can be obtained by straightforward geometrical analysis as

$$F = 1 - \left[\left(1 + \frac{2\, x_{dep}}{x_j}\right)^{\frac{1}{2}} - 1\right] \frac{x_j}{L}, \tag{25}$$

where x_j is the junction depth, x_{dep} is the thickness of various depletion regions, depending on the region of interest, and L is the effective channel length. Because of the nonuniform nature of the implanted profile, we have replaced it by a two-step profile (Fig. 2). Therefore, the integral in Eq. (24) contains not only contributions from the depletion charges in the bulk but also from ion implanted charges. In this case, the factor F defined in Eq. (25) has three different forms, F_s, F_d, and F, in the shallow implant, deep implant, and substrate depletion regions, respectively. This is shown in Fig. 4. The functional forms for F in the three regions are

$$F_s = 1 - \left[\left(1 + \frac{2\, W_S}{x_j}\right)^{\frac{1}{2}} - 1\right] \frac{x_j}{L}; \tag{26}$$

$$F_d = 1 - \left[\left(1 + \frac{2(W_S + W_B)}{x_j}\right)^{\frac{1}{2}} - 1\right] \frac{x_j}{L} + \left[\left(1 + \frac{2\, W_S}{x_j}\right)^{\frac{1}{2}} - 1\right] \frac{x_j}{L}; \tag{27}$$

$$F = 1 - \left[\left(1 + \frac{2\, x_{dm}}{x_j}\right)^{\frac{1}{2}} - 1\right] \frac{x_j}{L}, \tag{28}$$

where x_{dm} is the maximum depletion region, namely,

$$x_{dm} = \left[\frac{2\epsilon_s}{qN_X} (\phi_{so} + |V_{sx}| + \Delta V_{sx})\right]^{\frac{1}{2}}. \tag{29}$$

The variables N_X, ϕ_{so}, ΔV_{sx} are defined in Eqs. (13c), (13a), and (13e). The last term in Eq. (27) adds back the area originally removed in Eq. (26). This is because the deep implant does not extend to the surface region.

Now the effective depletion charge $Q_{d(eff)}$ in Eq. (24) can be written as follows.

1. For $|V_{sx}| < V_c$, the maximum depletion region thickness x_{dm} is located in the deep implant region. Thus

$$Q_{d(eff)} = (N_{AS} - N_{AB}) W_S F_S + N_X x_{dm} F. \quad (30)$$

2. For $|V_{sx}| \geq V_c$, the maximum depletion region thickness x_{dm} is located in the bulk substrate. Thus

$$Q_{d(eff)} = N_{AS} W_S F_s + N_{AB} W_B F_d + N_X x_{dm} F. \quad (31)$$

The threshold voltage equation can be written in the same form as in Eq. (13), namely

$$V_T = V_{FB} + \phi_{so} + \Delta V_T + F \frac{(2\epsilon_s q N_X)^{\frac{1}{2}}}{C_{ox}} (\phi_{so} + |V_{sx}| + \Delta V_{sx})^{\frac{1}{2}}. \quad (32)$$

However, a short channel factor, F, is added in the depletion charge term and a slight modification is needed in the ΔV_T term, i.e.,

$$\Delta V_T = \begin{cases} \dfrac{q(N_{AS} - N_{AB}) W_S}{C_{ox}} F_s & \text{for } |V_{sx}| < V_c, \\ \dfrac{qN_{AS} W_S}{C_{ox}} F_s + \dfrac{qN_{AB} W_B}{C_{ox}} F_d & \text{for } |V_{sx}| \geq V_c, \end{cases} \quad (33)$$

where V_c is defined in Eq. (12). In the Gaussian profile approximation, for $|V_{sx}| \geq V_c$, the threshold voltage has the same form as in Eq. (32) except that ΔV_T is replaced by

$$\Delta V_T = \frac{q\Phi_2}{C_{ox}} F_d + \frac{q\Phi_1}{2C_{ox}} \left[1 + \text{erf}\left(\frac{\bar{x}_1}{2^{\frac{1}{2}}\sigma_1}\right)\right] F_s, \quad (34)$$

and ΔV_{SX} is as defined in Eq. (23).

It can be easily seen that the short channel form factors approach unity for long channel length devices, $x_j \ll L$, and that the effective charge, $Q_{d(eff)}$ is equal to the total depletion charge Q_d obtained from the one-dimensional Poisson's equation. Actually, the surface potential along the channel is nonuniform due to the presence of the drain voltage, and therefore x_{dm} in Eq. (29) is also a function of the lateral voltage along the channel from source to drain. The approximation used in Eq. (29), which considers x_{dm} to be a constant, causes some error at large drain voltages. Because the drain voltage is always higher than the source voltage for an n-channel device, the depletion thickness at the drain is larger than that at the source. The reduction of depletion charges near the drain is more pronounced than at the source. Between the source and drain, the depletion region thickness varies as the square root of the surface potential. To avoid mathematical complexity, a term MV_D is added into the expression for x_{dm} to account for the drain voltage dependence of the short channel effect. Thus, the two-dimensional depletion region is replaced by a constant average drain-voltage-dependent depletion region, where the weighting factor M is taken to be equal to one-half. Thus, the depletion region thickness x_{dm} has a modified form that differs from the original one proposed by Poon, et al. [12] and Yau (13],

$$x_{dm} = \left[\frac{2\epsilon_s}{qN_X} (\phi_{so} + |V_{sx}| + \Delta V_{sx} + MV_D)\right]^{\frac{1}{2}} \quad (35)$$

The short channel form factor F for the bulk depletion charge given in Eq. (28) can be simply obtained by substituting Eq. (35) into Eq. (28).

As mentioned previously, for short channel MOSFETs the threshold voltage is in general a function of channel length, junction depth, and drain/source voltage. The simple models of Poon, et al. and Yau cannot illustrate the dependence of the threshold voltage on the drain voltage. Therefore, a modified short channel form factor is used by taking into account the average drain voltage across the depletion region. In this manner, a drain voltage dependence can be demonstrated in the threshold voltage equation.

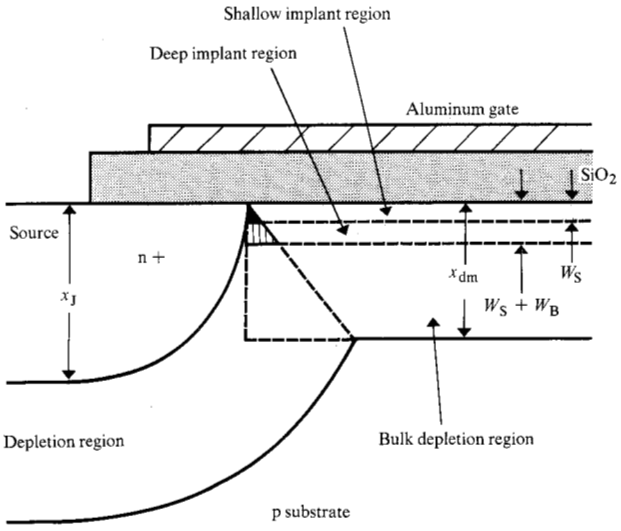

Figure 4 Short channel model of a double-boron-implanted structure by Poon and Yau. Dark triangle represents charge reduction of shallow implant region; shared trapezoidal portion is charge reduction of deep implant region; and dashed triangle shows charge reduction of bulk substrate region.

Experimental results and discussion

The devices for this study were fabricated in our laboratory. All the processing steps, such as oxidation, ion implantation drive-in, annealing, and aluminum metallurgy were done on a controlled MOSFET process line, utilizing the usual tests for process control. Several values used in the calculations came from separate pro-

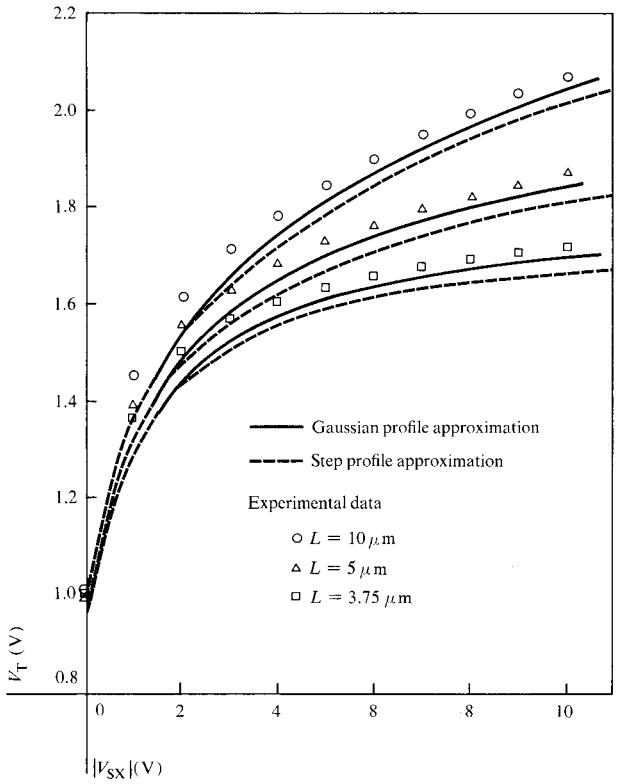

Figure 5 Substrate sensitivity curves of various channel length devices at $V_D = 0.1$ V.

cess measurements for this run. The well-known CV technique was used to determine most of these quantities. Range and straggle of the implant parameters were taken from a table adapted from the LSS theory [14]. Both automatic and bench testing were used in collecting the data. Many sites were tested, so the data are thought to be representative of the devices.

In accordance with most workers, the work function of aluminum to p-silicon was taken to be −0.85 V. From CV analysis, the following experimental parameters were found:

Substrate doping = $N_B = 1.4 \times 10^{15}$ atoms/cm^3;
Oxide thickness = $t_{ox} = 513$ Å;
Flat band voltage = $V_{FB} = -1.14$ V;
Effective oxide charge = $Q_{ox} = 1.04 \times 10^{11}$ charges/cm^2.

By a bevel and stain method, the junction depth x_j was found to be 1.7 μm.

Two implantations were made into the gate region. The deeper implant was used to increase the punch-through voltage of the device, allowing the use of a high resistivity substrate; the shallow one tailored the threshold voltage to the desired value. At a given deep implant dose, as the implanted energy increases, the punch-through voltage first increases, then falls to its nonimplanted value. At a given deep implant energy, as the implanted dose increases, the punch-through voltage first increases, then saturates and becomes almost independent of implanted ion dose. However, the deep implant increases the threshold voltage shift and the substrate sensitivity. Therefore, it is necessary to compromise between these two implants for optimium device design considerations. For our experimental conditions, a 15-Ω-cm p-type substrate with (100) orientation, the following implant parameters were used:

For punch-through: 2×10^{11} atoms/cm^2 at 150 keV;
For threshold: 6×10^{11} atoms/cm^2 at 35 keV.

The punch-through voltage is changed from about 8 V for a nonimplanted short channel device ($L \approx 3$ μm) to more than 20 volts for an implanted device.

The complexity of the resulting profile makes device characterization difficult. In studying the threshold voltage characteristics of these devices, we used two approximate techniques: a step profile and a Gaussian profile. We coupled these with the methods of Poon et al. [12] and of Yau [13] to include the short channel effect.

Modification of the short channel approach was necessary because of the complicated nature of the gate doping; in particular, a multiple correction factor depending on the doping region had to be included. Also the dependence on the drain voltage was included, but in a rather artificial manner.

In discussing the results, we denote the step profile and Gaussian approximations as SP and G, respectively. The short channel modification is included in all the calculated results. Figures 5-7 show how the techniques agree with each other and with experimental results. In these figures, the solid line always represents the results of the G approximation, the dashed line the SP approximation, and the circles represent experimental data.

Figure 5 shows the substrate sensitivity at $V_D = 0.1$ V for devices of different channel lengths. The effective channel lengths are electrically determined by comparing the variation of device transconductance with the photolithographic channel length. It can be seen from the figure that the functional forms of both the SP and the G curves agree well with the experimental points, but that the experimental values are larger than the calculations. This could result from a number of factors, the most obvious of which is the effective oxide charge. We chose to use the charge value determined from a monitor wafer that accompanied the device wafer. If we assume a slightly lower oxide charge of $Q_{ox} = 9.1 \times 10^{10}$ charges/cm^2, the G curve would move upward 30 mV, and its fit with experimental data would improve over most of the applicable range. The short channel model may also be a source of error. Although we adhered closely to the

concept of the Poon and Yau models, we feel that too much of the depletion charge near the source/drain is deducted in their approach, thereby excessively lowering the threshold voltage. Furthermore, our attempt to include a simple drain voltage correction is artificial, especially because the depletion region thickness does not vary linearly from source to drain but as the square root of the surface potential.

Note that in Fig. 5 the SP approximation is always lower than the G approximation value. Our method of choosing the doping values N_{AS} and N_{AB} as the averages over distances W_S and W_B, respectively, ignores the tail of the Gaussian distribution. This apparent dopant reduction has the effect of "turning on" the device at a lower gate potential. This could have been easily corrected if exact values were required, but we were chiefly concerned with functional variation. The G curve was calculated by assuming that the depletion region encompassed the implanted dopants; thus, for lower substrate voltages, there is a substantial deviation from experiment.

In general, the fit of theoretical to experimental data is quite good for the range of channel lengths considered. Even the flatter nature of the substrate sensitivity of the threshold voltage curve is well represented. Although the substrate voltage range has to be broken into two different regions to use the SP approximation, results are easily obtained. In our case, the calculations were performed using APL, but any calculational computer language could be used.

Essentially the same behavior is seen for Figs. 6 and 7, which show the variation of V_T with L for two different drain voltages, $V_D = 0.1$ V and $V_D = 5$ V. Both are for a substrate voltage of 5 V. In any case, the G approximation matches the experimental points better than does the SP approximation. Shifting the calculated curves upward by adjusting the oxide charge or some other parameter would result in better agreement for $V_D = 0.1$ V but would not improve matters for $V_D = 5$ V. This is due to the function difference at higher drain voltages caused by the short channel effect.

Acknowledgment

The authors express their appreciation to various departmental colleagues for stimulating and provocative discussions on pertinent matters, especially to T. A. Larsen and T. J. Murphy for their continuous interest and encouragement throughout the course of this work. They are also grateful to R. Rehfeld for laboratory support.

Appendix: One-dimensional Poisson's equation for nonuniform doping profile

Consider an MOS structure with a nonuniform doping concentration, $C(x)$, with $x = 0$ corresponding to the oxide-silicon interface. The bulk material has a constant ion concentration N_B and is taken as the reference level for the potential $\phi(x)$, i.e., $\phi = 0$ in the bulk. Surface potential is ϕ_s.

From Poisson's equation and the depletion approximation, one obtains [17]

$$\frac{d\phi}{dx} = \frac{q}{\epsilon_s}\int_0^x C(x)\,dx + \left(\frac{d\phi}{dx}\right)_{x=0}; \tag{A1}$$

$$\phi(x) = \frac{q}{\epsilon_s}\int_0^x \int_0^u C(v)\,dv du + x\left(\frac{d\phi}{dx}\right)_{x=0} + \phi_s \tag{A2}$$

Because the charge neutrality condition is assumed for $x \geq x_d$, the depletion edge, we can arrive at the surface potential ϕ_s in the following form:

$$\phi_s = \phi(x_d) - x_d\left(\frac{d\phi}{dx}\right)_{x=x_d} + \frac{q}{\epsilon_s}\int_0^{x_d} x\,C(x)\,dx, \tag{A3}$$

where

$$\phi(x_d) = \frac{kT}{q}\ln\left(\frac{N_B}{C(x_d)}\right). \tag{A4}$$

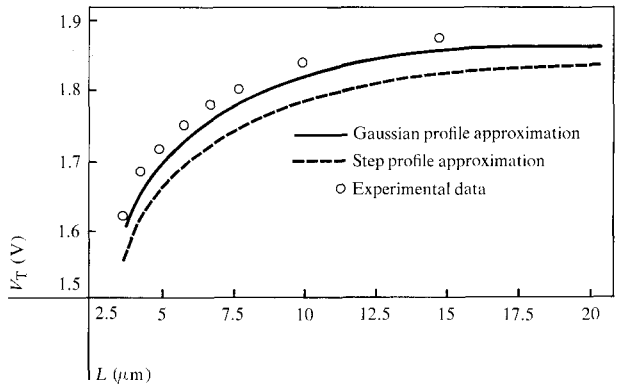

Figure 6 V_T vs L at $V_D = 0.1$ V and $|V_{sx}| = 5$ V.

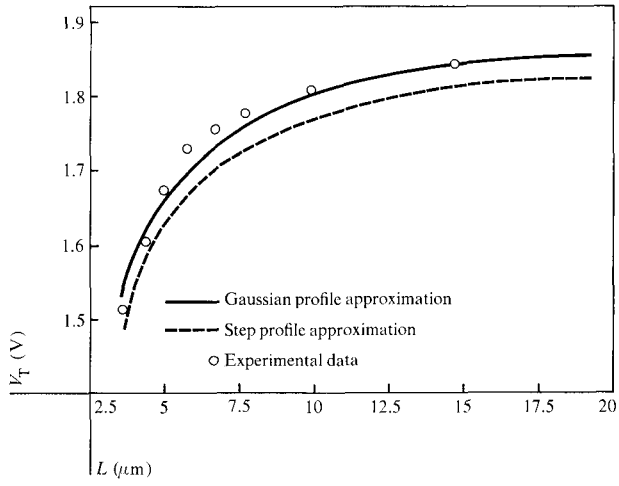

Figure 7 V_T vs L at $V_D = 5$ V and $|V_{sx}| = 5$ V.

The criterion for strong inversion is

$$\phi_{s(inv)} = \phi_{bi} + |V_{sx}|, \tag{A5}$$

where $|V_{sx}|$ is the source-to-substrate voltage and

$$\phi_{bi} = \frac{kT}{q} \ln\left(\frac{C(x_{dm})\ N_B}{n_i^2}\right), \tag{A6}$$

in which x_{dm} is the maximum depletion region width.

By substituting Eq. (A5) into Eq. (A3), we determine that x_{dm} is satisfied by the following equation:

$$\phi_{so} + |V_{sx}| = -\ x_{dm}\left(\frac{d\phi}{dx}\right)_{x_{dm}} + \frac{q}{\epsilon_s}\int_0^{x_{dm}} x\ C(x)\ dx, \tag{A7}$$

where

$$\phi_{so} = (2kT/q)\ \ln\left[C(x_{dm})/n_i\right] \tag{A8}$$

is the intrinsic band bending at the silicon surface at the onset of strong inversion. The threshold voltage equation at the onset of strong inversion is

$$V_T = V_{FB} + \phi_{so} + V_{bulk}, \tag{A9}$$

where

$$V_{bulk} = \frac{q}{C_{ox}}\int_0^{x_{dm}} C(x)\ dx. \tag{A10}$$

In the case of a uniform doping profile, $C(x) = N_B$, Eq. (A2) reduces to

$$\phi_{so} + |V_{sx}| = \frac{q}{2\epsilon_s} N_B\ x_{dm}^2. \tag{A11}$$

Again, from Eq. (A10) we have

$$V_{bulk} = \frac{qN_B x_{dm}}{C_{ox}} = \frac{(2\epsilon_s q N_B)^{\frac{1}{2}}}{C_{ox}}\ (\phi_{so} + |V_{sx}|)^{\frac{1}{2}}, \tag{A12}$$

and the threshold voltage from Eq. (A9) yields

$$V_T = V_{FB} + (2kT/q)\ \ln\ (N_B/n_i) + \frac{(2\epsilon_s q N_B)^{\frac{1}{2}}}{C_{ox}}\ (\phi_{so} + |V_{sx}|)^{\frac{1}{2}}. \tag{A13}$$

References

1. M. R. MacPherson, "Threshold Shift Calculations for Ion Implanted MOS Devices," *Solid-State Electron.* **15,** 1319 (1972).
2. M. Kamoshia, "Threshold Voltage and Gain Beta of Ion Implanted Enhancement Mode N-Channel MOS Transistors," *Appl. Phys. Lett.* **22,** 404 (1973).
3. M. Kamoshia, "Electrical Characteristics of Boron Implanted N-Channel MOS Transistors," *Solid-State Electron,* **17,** 621 (1974).
4. R. H. Dennard, F. H. Gaenaalen, H. N. Yu, V. L. Rideout, E. Bassous, and A. R. LeBlanc, "Design of Ion Implanted MOSFET's with Very Small Physical Dimensions," *IEEE J. Solid-State Circuits* **SC-9,** 256 (1974).
5. V. L. Rideout, F. H. Gaensslen, and A. R. LeBlanc, "Device Design Considerations for Ion Implanted N-Channel MOSFET's," *IBM J. Res. Develop.* **19,** 50 (1975).
6. P. P. Peressini and W. S. Johnson, "Threshold Adjustment of N-Channel Enhancement Mode FETs by Ion Implantation," *1973 IEDM Digest,* 467 (1973).
7. K. H. Christie and W. S Johnson, "N-Channel MOSFET Field Protection by Non-Masked Boron Ion Implantation," *1973 IEDM Digest,* 464 (1973).
8. W. S. Johnson, P. P. Peressini, and K. H. Christie, "Design of Short Channel Ion Implanted MOSFETs with Relatively Deep Junctions," *1974 IEDM Digest,* 550 (1974).
9. M. B. Barron, "Computer Aided Analysis of Insulated Gate Field Effect Transistors," *Report # 5501-1,* Stanford Electronics Laboratories, Stanford, Calif., 1969.
10. D. P. Kennedy and P. C. Murley, "Steady State Mathematical Theory for the Insulated Gate Field Effect Transistor," *IBM J. Res. Develop.* **17,** 1 (1973).
11. M. S. Mock, "A Two-Dimensional Mathematical Model of the Insulated Gate Field Effect Transistor," *Solid-State Electron.* **16,** 601 (1973).
12. H. C. Poon, L. D. Yau, R. L. Johnson, and D. Beecham, "D. C. Model for Short-Channel IGFET's," *1973 IEDM Digest,* 156 (1973).
13. L. D. Yau, "A Simple Theory to Predict the Threshold Voltage of Short Channel IGFET's," *Solid-State Electron.* **17,** 1059 (1974).
14. G. Dearnaley, J. H. Freeman, R. S. Nelson, and J. Stephen, *Ion Implantation,* American Elsevier Publishing Company, New York, 1973, p. 39.
15. J. F. Gibbons, "Ion Implantation in Semiconductors, Part I: Range Distribution Theory and Experiments," *Proc. IEEE* **56,** 295 (1968).
16. V. G. K. Reddi and A. Y. C. Yu, "Ion Implantation for Silicon Device Fabrication," *Solid State Technol.* (October 1972).
17. G. Doucet and F. Van de Wiele, "Threshold Voltage of Nonuniform Doped MOS Structures," *Solid-State Electron,* **16,** 417 (1973).
18. H. S. Lee, "An Analysis of Threshold Voltage for Short Channel IGFETs," *Solid-State Electron.* **16,** 1407 (1973).
19. H. S. Lee, "Threshold Voltage of Short Channel IGFET," *Semiconductor Silicon 1973,* edited by H. R. Huff and R. R. Burgess, Electrochemical Society Inc., Princeton, N.J., 1973, pp 791-801.

Received March 24, 1975; revised July 21, 1975

The authors are located at the IBM System Communications Division Laboratory, Kingston, NY 12401.